Chapter 3

Combinatorial Doping of TiO_2 with Platinum (Pt), Chromium (Cr), Vanadium (V), and Nickel (Ni) to Achieve Enhanced Photocatalytic Activity with Visible Light Irradiation

The text of this chapter has been accepted for publication in *Journal of Materials Research* Choi, J.; Park, H.; Hoffmann, M.R. July 2009.

Abstract

Titanium dioxide (TiO_2) was doped with the combination of several metal ions including platinum (Pt), chromium (Cr), vanadium (V), and nickel (Ni). The doped TiO_2 materials were synthesized by standard sol-gel methods with the doping levels of 0.1 to 0.5 atom-%. The resulting materials were characterized by the X-ray diffraction (XRD), BET surface-area measurement, Scanning Electron Microscopy (SEM), and UV-Vis diffuse reflectance spectroscopy (DRS). The visible-light photocatalytic activity of the co-doped samples was quantified by measuring the rate of the oxidation of iodide, the rate of degradation of methylene blue (MB), and the rate of oxidation of phenol in aqueous solutions at $\lambda > 400$ nm. 0.3 atom-% Pt-Cr-TiO_2 and 0.3 atom-% Cr-V-TiO_2 showed the highest visible-light photocatalytic activity with respect to MB degradation and iodide oxidation, respectively. However, none of the co-doped TiO_2 samples were found to have enhanced photocatalytic activity for phenol degradation when compared to their single-doped TiO_2 counterparts.

Introduction

Titania (TiO_2) is the most widely used photocatalyst for the purification of water, air, and other environmental application because of its high photocatalytic activity, excellent chemical stability, relatively low price, and its lack of any known toxicity. Redox reactions of environmental interest are initiated on the TiO_2 surface with trapped electrons and holes after band-gap excitation. However, because of its wide band gap energy of ~3.2 eV, TiO_2 is active only in the ultraviolet portion of the solar spectrum. As a consequence, significant efforts have been made to develop modified forms of TiO_2 that are active under visible-light ($\lambda > 400$ nm) irradiation. Several different strategies have been employed to extend photoactivity into the visible region. They include (i) doping with anions (e.g., nitrogen,[1-3] sulfur,[4] iodine,[5-7] and fluorine[8]), (ii) doping with metal ions,[9-18] and (iii) functionalizing TiO_2 with photo-sensitizers that absorb visible-light.[19,20]

The most actively pursued strategy has been to increase the photoactive wavelength range and to enhance the photocatalytic activity under UV irradiation by metal ion-doping of TiO_2.[21-23] Numerous metal ions have been investigated as potential dopants while several metal ions such as iron,[9-11] vanadium,[12-14] chromium,[15,16] nickel,[17] and platinum[18] have been reported to show visible-light photocatalytic activity.

In addition, efforts have been made to improve the visible-light photocatalytic activity of TiO_2 by co-doping with two metal ions.[24-28] Ahmad et al. reported that Sc and Nb co-doped TiO_2 nanoparticles are relatively more photoactive for 2-chlorophenol degradation under visible-light than the particles doped with Sc or Nb alone.[25] Kato and Kudo showed that TiO_2 co-doped with Sb^{5+} and Cr^{3+} ions showed higher activity than TiO_2 doped only with Cr^{3+} ions alone for O_2 evolution because of the charge compensation achieved with

Sb^{5+} doping.[26] Furthermore, TiO_2 co-doped with Ni^{2+} and Ta^{5+} (or $Ni^{2+}$and Nb^{5+}) and TiO_2 co-doped with $Rh^{3+}$and Sb^{5+} were also shown to improve photocatalytic activity for O_2 evolution under visible-light irradiation.[27,28] However, there have been relatively few studies reported for double metal ion co-doping of TiO_2, while TiO_2 co-doped with two nonmetallic elements (e.g., N and F co-doping,[29,30] N and S co-doping[31,32]) or with metal ions and nonmetallic elements[33-39] (e.g., Cr and N co-doping[35] Pt and N co-doping,[36] V and N co-doping,[37] and Bi and S co-doping[38]) have been widely investigated.

In order to examine the efficacy of double-doping with metal ions, we have prepared co-doped TiO_2 with Pt^{4+} (or Pt^{2+}), Cr^{3+}, V^{3+}, and Ni^{2+} ions and characterized their physicochemical properties and photocatalytic activities for the bleaching and degradation of methylene blue (MB), the oxidation of iodide to tri-iodide, and the oxidative degradation of phenol in aqueous solution under visible-light irradiation ($\lambda >$ 400 nm).

Experimental

Sample Preparation

TiO_2 nanoparticles were prepared by standard sol-gel methods. 5.0 mL of titanium tetraisopropoxide (TTIP, Aldrich) was dissolved in 50 mL of absolute ethanol (Mallinckrodt) and then added dropwise to 50 mL of distilled water adjusted to pH 1.5 with nitric acid under vigorous stirring at room temperature. After 24 hours, the resulting transparent colloidal suspensions were evaporated using a rotary evaporator at 45 ^oC and dried in the oven (70 ^oC) overnight. The resulting powders were calcined at 400 ^oC for 1 hour under air. Single or double-doped TiO_2 samples (M-TiO_2 or MM-TiO_2) were

prepared by adding one or two metal precursors to the distilled water prior to the hydrolysis of TTIP to give a doping level from 0.1 to 0.5 atomic % (at.%). Platinum (Pt^{4+} and Pt^{2+}), chromium (Cr^{3+}), vanadium (V^{3+}), and nickel (Ni^{2+}) were selected as metal-ion dopants in this study. $PtCl_4$ (Aldrich), $Pt(NH_3)_4(NO_3)_2$ (Alfar Aesar), $Cr(NO_3)_3 \cdot 9H_2O$ (Aldrich), VCl_3 (Aldrich), and $Ni(NO_3)_2 \cdot 6H_2O$ (Alfar Aesar) were used as precursor reagents. Six different TiO_2 samples were synthesized and co-doped with (i) Pt^{4+} and Cr^{3+} ions (Pt(IV)-Cr-TiO_2), (ii) Pt^{2+} and Cr^{3+} ions (Pt(II)-Cr-TiO_2), (iii) Cr^{3+} and V^{3+} ions (Cr-V-TiO_2), (iv) Pt^{2+} and V^{3+} ions (Pt(II)-V-TiO_2), (v) Pt^{2+} and Ni^{2+} ions (Pt(II)-Ni-TiO_2), and (vi) Cr^{3+} and Ni^{2+} ions (Cr-Ni-TiO_2). In addition, a control sample without doping was prepared along with singly-doped TiO_2 (i.e., Pt(IV)-TiO_2, Pt(II)-TiO_2, Cr-TiO_2, V-TiO_2, and Ni-TiO_2) for comparison with co-doped TiO_2.

Characterization

We used X-ray diffraction (XRD) to examine the crystal structures of synthesized TiO_2 particles by using a Philips diffractometer (X'pert Pro) with Cu-Kα radiation. Brunauer-Emmett-Teller (BET) surface area measurement was carried out by using N_2 as the adsorptive gas (Micromeritics Gemini series). Scanning electron microscopic images (SEM, LEO 1550VP model) were taken to investigate the morphology of TiO_2 particles and analysis of elemental composition was also performed with EDS (Energy Dispersive X-ray Spectroscopy). Diffuse reflectance UV-Vis absorption spectra (DRS) of powder samples were obtained using UV-Vis spectrometer (Shimadzu UV-2101PC) equipped with a diffuse reflectance accessory.

Photocatalytic Activity Measurements

Photocatalytic activities of the synthesized TiO_2 samples were quantified with respect to rates of photo-bleaching and degradation of Methylene Blue (MB), the rates of oxidation of iodide (I^-), and the rates of oxidative degradation of phenol (PhOH). The individual photocatalyst powders were dispersed in distilled water to give a mass concentration of 1 g L^{-1}. An aliquot of the target substrate stock solution was then added to the catalyst suspension to give the specific substrate concentration (e.g., $[MB]_0$ = 10 μM, $[I^-]_0$ = 50 mM, and $[PhOH]_0$ = 50 μM). The reaction suspension pH was circum-neutral. Before irradiation, the suspension was stirred in the dark for 30 min to obtain a state of sorption equilibrium of the specific substrate on TiO_2.

A high-pressure Hg(Xe) Arc lamp (500 W) was used as the light source. The light beam emitted from the arc lamp was passed through an IR water filter and a UV cut-off filter ($\lambda > 400$ nm) before being focused onto a cylindrical Pyrex reactor through a quartz window. The reactor was open to ambient air during most experiments. Time-sequenced sample aliquots were collected from the reactor during the illumination for analysis and filtered through a 0.45 μm PTFE syringe filter to remove the TiO_2 particles. Multiple photolysis (and photocatalysis) experiments were performed under identical reaction conditions to determine reproducibility.

The degradation rates and rate constants for MB loss during photocatalysis were determined by measuring the absorbance of MB at 665 nm with a spectrophotometer (Shimadzu UV-2101PC). For the photocatalytic oxidation of I^-, tri-iodide (I_3^-), which is the principal product of I^- oxidation in the presence of excess iodide ion, was spectrophotometrically determined by measuring the absorbance at 352 nm. The

degradation of phenol in aqueous solution was measured using high performance liquid chromatography (HPLC, HP 1100 series with C18 column).

Results and Discussion

Characterization of Single Metal Doped TiO_2 (M-TiO_2)

Singly-doped TiO_2 (M-TiO_2) samples were prepared by sol-gel synthesis where M = Pt^{4+}, Cr^{3+}, V^{3+}, and Ni^{2+}. In order to compare the effect of oxidation state of Pt dopant, TiO_2 doped with Pt^{2+} ions was also prepared. Figure 3.1 shows the XRD patterns of the singly-doped M-TiO_2 samples at the doping level of 0.3 at.%. The XRD patterns were consistent with the standard crystal structure of TiO_2 (i.e., a mixture of anatase and rutile phases) with no diffraction peaks associated with any of doped metals elements in the M-TiO_2 samples. This indicates that the doping process did not induce the formation of separate impurity phases and that the specific dopant could be considered to be fully incorporated into TiO_2 lattice. Pt^{4+}, Cr^{3+}, and V^{3+} ions may be substituted into Ti site of TiO_2 because the ionic radii of dopants (Pt^{4+}: 0.765 Å, Cr^{3+}: 0.755 Å, and V^{3+}: 0.78 Å)[40] are similar to that of Ti^{4+} (0.745 Å).[40] However, Ni^{2+} and Pt^{2+} ions are possibly located in the interstitial position of the lattice rather than Ti site because of relatively large size difference between dopant ions (Ni^{2+}: 0.83 Å and Pt^{2+}: 0.94 Å)[40] and Ti^{4+} ions. Undoped TiO_2 samples prepared by sol-gel synthesis and calcined at 400 ^oC (TiO_2-SG) showed only the pure anatase phase. However, the rutile phase was apparent in some M-TiO_2 samples prepared and treated at the same temperature. This result suggests that metal-ion doping lowered relative temperature of the anatase-to-rutile phase transformation (A-R phase transformation). 0.3 at.% Cr-TiO_2 and 0.3 at.% Pt-TiO_2 (both Pt(IV)-TiO_2 and

Pt(II)-TiO_2) exhibited a characteristic rutile peak whereas 0.3 at.% V-TiO_2 appeared to have a smaller fraction of the rutile phase. 0.3 at.% Ni-TiO_2, by contrast, showed pure anatase phase, as in the case of undoped TiO_2. Therefore, we conclude that doping TiO_2 with Cr, Pt, and V ions modifies the temperature dependence of the A-R phase transformation.

Figure 3.2 shows the UV/vis diffuse-reflectance spectra for the various M-TiO_2 samples. Undoped TiO_2 exhibited a sharp absorption edge at about 400 nm (E_{bg} ~ 3.1 eV). However, the M-TiO_2 samples showed absorption spectra extended into the visible region over the range of 400 ~ 700 nm. Thus, visible-light activation and photocatalytic activity could be expected from these M-TiO_2 samples. As shown in Figure 3.2a, 0.3 at.% Ni-TiO_2 gave a relatively small absorption between 400 and 500 nm while 0.3 at.% V-TiO_2 exhibited a more substantial and broader absorption shoulder up to 700 nm. 0.3 at.% Cr-TiO_2 also showed extended absorption spectra over the 400~500 nm range with an additional absorption peak near 650 nm; this may be due to the d-d transitions of Cr^{3+} ions.[26,41] Figure 3.2b shows the difference between the absorption spectra of 0.3 at.% Pt(IV)-TiO_2 and 0.3 at.% Pt(II)-TiO_2. Pt(II)-TiO_2 gave a broad absorption over most of the visible region similar to 0.3 at.% V-TiO_2. In contrast, 0.3 at.% Pt(IV)-TiO_2 gave a smaller absorption peak between 400 and 550 nm; this indicates that the origins of the absorption spectra were different in the two different Pt-TiO_2 samples. The extended absorption of the M-TiO_2 into the visible region has been explained in terms of the excitation of electrons of dopant ion to TiO_2 conduction band (i.e., a metal to conduction band charge-transfer) according to their respective energy levels.[12,13,42,43] However, recent proposals suggest that the absorption spectra of modified TiO_2 in the visible region

most likely originate from defects associated with oxygen vacancies that give rise to colored centers.[44,45] Kuznetsov and Serpone pointed out the similarities of the spectra in the range of 400~600 nm shown among different types of visible-light-active TiO_2 samples.[44] It was also reported that similar absorption spectra in the visible region was found in reduced TiO_2 samples with observed absorption spectra being the sum of overlapping absorption bands with the maxima at 2.81 eV and 2.55 eV, which correlate with oxygen vacancies.[46,47] The metal-ion dopants used in this study have different valence states than Ti^{4+}, and as a consequence, may induce the generation of oxygen vacancies during synthesis. In addition, some of the M-TiO_2 samples (e.g., Ni-TiO_2, V-TiO_2, Pt(II)-TiO_2) exhibited similar absorption in the range of 400~600 nm, even though the absorption intensities were different. Therefore, both the generation of new energy levels due to the injection of impurities within the bandgap energies range and the generation of oxygen vacancies by metal doping may contribute to the observed visible light absorption of M-TiO_2 samples.

Characterization of metal co-doped TiO_2 (MM-TiO_2)

The properties of 0.3 at.% MM-TiO_2 samples are summarized in Table 3.1. The doubly-doped MM-TiO_2 samples exhibited a variety of colors; TiO_2 samples doped with Cr or Ni are green; Pt doped samples are brown; and V doped samples are orange. The BET surface area of the sol-gel synthesized, undoped TiO_2, which was calcined at 400 ^oC, was determined to be 104 cm^2/g, whereas surface area of Degussa P25 TiO_2 was measured at 50 cm^2/g, indicating that the TiO_2 particles synthesized by sol-gel methods have substantially higher surfaces areas and adsorption capacities per unit weight than

Degussa P25. The surface areas of 0.3 at.% M-TiO_2 samples were found to be slightly larger than the undoped TiO_2 (106 ~ 132 cm^2/g). However, there were no significant increases in the surface areas of doubly-doped samples (~110 cm^2/g).

XRD patterns of 0.3 at.% Pt(IV)- 0.3 at.% Cr-TiO_2 and 0.3 at.% Cr-0.3 at.% Ni-TiO_2 are shown in Figure 3.3 with XRD patterns of each singly-doped TiO_2. Crystal structures of all MM-TiO_2 samples are also listed in Table 3.1 along with the BET surface areas. Figure 3.3a shows that a rutile phase of Cr or Pt singly-doped TiO_2 was well maintained in doubly-doped Pt(IV)-Cr-TiO_2 samples. In Figure 3.3b, however, 0.3 at.% Cr-0.3 at.% Ni-TiO_2 sample appeared to lack evidence for a rutile phase that was clearly shown in singly-doped 0.3 at.% Cr-TiO_2. Similarly, 0.3 at.% Pt(II)- 0.3 at.% Ni-TiO_2 appeared to be a pure anatase phase material in spite of 0.3 at.% Pt(II) doping. Therefore, we suggest that co-doping with Ni ions may inhibit the A-R phase transformation in Cr-TiO_2 or Pt-TiO_2.

For comparison, the fraction of rutile, X_R, was calculated from the respective peak intensities using the following equation:[48]

$$X_R\,(\%) = \{1- (1 + 1.26I_R/I_A)^{-1}\} \times 100 \qquad (3.1)$$

where I_R and I_A are the X-ray intensities of the rutile (101) and anatase (110) peaks, respectively. These relative rutile fractions are listed in Table 3.1. These results show that the fraction of rutile (X_R) in MM-TiO_2 was not higher than that for each of M-TiO_2 samples. For example, X_R of 0.3 at.% Pt(IV)-Cr-TiO_2 was estimated to be 32% while X_R of 0.3 at.% Pt(IV)-TiO_2 and 0.3 at.% Cr-TiO_2 were estimated as 26% and 34%, respectively. Furthermore, 0.3 at.% Pt(II)- 0.3 at.% V-TiO_2 and 0.3 at.% Cr-0.3 at.% V-

TiO_2 had similar or lesser X_R values than those of 0.3 at.% Pt(II)-TiO_2, 0.3 at.% V-TiO_2, or 0.3 at.% Cr-TiO_2.

Figure 3.4 shows SEM images of 0.3 at.% Pt-0.3 at.% Cr-TiO_2. In Figure 3.4a, 0.3 at.% Pt(IV)- 0.3 at.% Cr-TiO_2 particles were aggregated together and showed rough morphologies. 0.3 at.% Pt(II)- 0.3 at.% Cr-TiO_2 (Figure 3.4b) and other MM-TiO_2 (images were not shown here) also showed SEM images similar to 0.3 at.% Pt(IV)- 0.3 at.% Cr-TiO_2. Niishiro et al. reported that doping with Sb^{3+} ions in TiO_2 suppressed sintering due to the difference in size between Sb^{3+} (0.90 Å) and Ti^{4+}, which resulted in the formation of finer and smoother crystalline particles.[28] However, in our case, the doping of 0.3 at.% Pt^{2+} (0.94 Å) did not significantly change either the size of particle or their morphologies (Figure 3.4b). This may be due to relatively low doping level (0.3 % vs. 0.5~2 %) and a lower calcination temperature (400 ^oC vs. 1150 ^oC). In addition, the EDS spectrum of 0.3 at.% Pt(II)- 0.3 at.% Ni-TiO_2 (Figure 3.4c) shows that no apparent signals for Pt and Ni; only those of Ti and O were observed. This indicates that metal ions with larger ionic radii than Ti^{4+} such as Pt^{2+} or Ni^{2+} ions are well incorporated into the TiO_2 lattice and not located in the surface region; these results are consistent with XRD results.

There were no significant differences between 0.3 at.% Pt(IV)- 0.3 at.% Cr-TiO_2 and 0.3 at.% Pt(II)- 0.3 at.% Cr-TiO_2 in terms of the XRD pattern, BET surface areas, morphology, or element analysis as determined by EDS. However, UV/vis DRS results clearly show the difference between two samples, as shown in Figure 3.5. 0.3 at.% Pt(IV)- 0.3 at.% Cr-TiO_2 shows an enhanced absorption compared to 0.3 at.% Pt-TiO_2 or 0.3 at.% Cr-TiO_2. The spectral response of 0.3 at.% Pt(IV)- 0.3 at.% Cr-TiO_2 appears to

be an additional spectrum of the singly-doped 0.3 at.% Pt-TiO_2 combined with that of 0.3 at.% Cr-TiO_2 (Figure 3.5a). On the other hand, the absorption of 0.3 at.% Pt(II)- 0.3 at.% Cr-TiO_2 was almost identical to 0.3 at.% Cr-TiO_2 (Figure 3.5b). Therefore, we could expect that absorption of visible light is more efficient in the 0.3 at.% Pt(IV)- 0.3 at.% Cr-TiO_2 samples than the singly-doped 0.3 at.% Pt(IV)-TiO_2 samples.

Figure 3.6 shows UV/vis DRS results for other doubly-doped MM-TiO_2 materials. The absorption spectra of the 0.3 at.% Pt(II)- 0.3 at.% V-TiO_2 sample (Figure 3.6a) and the 0.3 at.% Pt(II)- 0.3 at.% Ni-TiO_2 sample (Figure 3.6b) were the same as those of the 0.3 at.% singly-doped V-TiO_2 and Ni-TiO_2 samples, respectively. In all the cases of Pt(II)-M-TiO_2, the Pt(II) did not attribute to the absorption spectra of the co-doped TiO_2. In contrast, Pt(IV) was the only effective co-dopant for enhanced visible-light absorption in the Cr-M-TiO_2 samples. For example, 0.3 at.% Cr-0.3 at.% Ni-TiO_2 (Figure 3.6c) and 0.3 at.% Cr-0.3 at.% V-TiO_2 (Figure 3.6d) did not show enhanced absorption compared to the sum of singly-doped TiO_2, while 0.3 at.% Cr-0.3 at.% Pt(IV)-TiO_2 has a significantly enhanced absorption in the visible region (Figure 3.5a).

Visible-light Photocatalytic Activity

Figure 3.7 shows visible-light photocatalytic activities of various M-TiO_2 and MM-TiO_2 preparations for the degradation of methylene blue (MB) in aqueous solution. The degradation and bleaching reaction followed apparent first-order kinetics. Under visible-light irradiation at $\lambda > 400$ nm, direct photolysis of MB was observed in the absence of TiO_2 particles since MB molecules can absorb visible-light and become photolyzed without the photocatalyst. The measured first-order rate constant, k_{MB}, was increased

slightly in the presence of undoped TiO_2. This increase may be due to additional light absorption above 400 nm by the TiO_2 particles or by an enhanced electron transfer from MB to the conduction band of TiO_2. All the singly-doped M-TiO_2 preparations showed visible-light photocatalytic activities for MB degradation while the 0.3 at.% Pt(II)-TiO_2 samples gave the highest values for k_{MB}. Among doubly-doped MM-TiO_2 samples, only 0.3 at.% Pt-0.3 at.% Cr-TiO_2 (both Pt(IV) and Pt(II)) and Pt(II)-Ni-TiO_2 showed higher k_{MB} values than those measured for the singly-doped TiO_2 samples. Therefore, co-doping with Pt appears to be effective for enhancing the visible-light degradation of MB degradation. On the other hand, the doubly-doped Pt-V-TiO_2 samples had lower photocatalytic activity, which may be due to the effect of V doping.

0.3 at.% Pt(IV)- 0.3 at.% Cr-TiO_2, which has enhanced visible-light absorption (Figure 3.5a), proved to be less photo-active than 0.3 at.% Pt(II)- 0.3 at.% Cr-TiO_2. On the other hand, 0.3 at.% Cr-0.3 at.% V-TiO_2 and 0.3 at.% Pt(II)- 0.3 at.% V-TiO_2 had significantly decreased k_{MB} values compared to their singly-doped TiO_2 counterparts. In comparison to the 0.3 at.% Cr-0.3 at.% Ni-TiO_2 and 0.3 at.% Pt(II)- 0.3 at.% Ni-TiO_2 samples, V co-doping of Cr-TiO_2 and Pt-TiO_2 showed a net negative effect on photocatalytic activity. However, these samples still showed better photocatalytic activity than undoped TiO_2.

The photocatalytic oxidation of iodide ions (I^-) can also be used to compare the visible-light photocatalytic activities of various MM-TiO_2 preparations. Iodide in aqueous solution is readily oxidized to tri-iodide (I_3^-) according to the following reaction:

$$I^- + h_{vb}^+ \longrightarrow I\cdot \xrightarrow{+I\cdot} I_2 \xrightarrow{+I^-} I_3^-$$

Figure 3.8 shows the production of I_3^- ions from I^- oxidation under visible-light irradiation in the presence of doubly-doped MM-TiO_2 materials. As a control measurement, no I_3^- was produced in the absence of TiO_2 particles at $\lambda > 400$ nm. Undoped TiO_2, 0.3 at.% V-TiO_2, and 0.3 at.% Pt(II)-TiO_2 showed little photo-catalytic activity with respect to the net photooxidation of I^- to I_3^-. However, 0.3 at.% V-0.3 at.% Cr-TiO_2 and 0.3 at.% Pt(II)- 0.3 at.% Cr-TiO_2 had higher photoactivities. Therefore, Cr is clearly an effective co-dopant with respect to I^- photo-oxidation in the visible. I_3^- production is very fast during the initial phases of the reaction, but it slows noticeably as irradiation continues. This is due to the back photo-reaction of I_3^- with conduction band electrons to reform I^- ions. The back reaction effectively competes with the forward reaction of iodide with valence-band holes or surface hydroxyl radicals as the concentration of I_3^- increases with time.

In Figure 3.9, the photo-catalytic activities of the singly-doped M-TiO_2 samples and the doubly-doped MM-TiO_2 samples are compared in terms of total amount of I_3^- ions produced during 15 min of irradiation. Similar to MB degradation, all the M-TiO_2 samples improved the I^-oxidation rates; 0.3 at.% Pt(IV)-TiO_2 and 0.3 at.% Cr-TiO_2 showed the highest activity. However, 0.3 at.% Pt(II)-TiO_2, 0.3 at.% V-TiO_2, and 0.3 at.% Ni-TiO_2, which had comparable activities to 0.3 at.% Pt(IV)-TiO_2 or 0.3 at.% Cr-TiO_2 in terms of MB degradation, showed only slightly enhanced I^- oxidation rates. Most of MM-TiO_2 samples also showed some enhanced photocatalytic activity. 0.3 at.% Pt(II)-0.3 at.% V-TiO_2 had the least visible-light activity among the doubly-doped MM-TiO_2 samples.

The doping level of each dopant in Pt(II)-Cr-TiO_2 was also optimized. Table 3.2 shows photocatalytic activities of Pt(II)-Cr-TiO_2 with different concentration of Pt and Cr over the range of 0.1~0.5 atom-%. The optimal concentration for increased photocatalytic activity was found to be 0.3 at.% Pt(II) and 0.3 at.% Cr, respectively. It was also observed that photocatalytic activity with respect to I^- oxidation strongly depended on Cr concentration.

The photocatalytic degradation of phenol under visible-light irradiation is shown in Figure 3.10. Phenol was degraded effectively with Pt-TiO_2 (both Pt(IV)-TiO_2 and Pt(II)-TiO_2) and totally degraded within 2 hr with 0.3 at.% Pt(IV)-TiO_2. However, 0.3 at.% Pt-0.3 at.% Cr-TiO_2 did not exhibit any enhancement in the photo-degradation of phenol (Figure 3.10a). Phenol degradation with 0.3 at.% Pt(IV)-TiO_2 was slightly decreased by Cr co-doping. Moreover, the resultant photocatalytic activity of 0.3 at.% Pt(II)- 0.3 at.% Cr-TiO_2 proved to be much less than 0.3 at.% Pt(II)-TiO_2. Similarly, there was no advantage shown by the doubly-doped Cr-V-TiO_2 samples (Figure 3.10b). The other doubly-doped MM-TiO_2 samples, which are not shown here, also had negative co-doping effects with respect to phenol degradation. These results clearly indicate that the co-doping effects on TiO_2 photo-catalytic activity are substrate-dependent. Several doubly-doped MM-TiO_2 samples showed enhanced photocatalytic activities for MB degradation or I^- oxidation. For example, 0.3 at.% Pt(II)- 0.3 at.% Cr-TiO_2 and 0.3 at.% Cr-0.3 at.% V-TiO_2 showed the highest visible-light photocatalytic activities for MB degradation and I^- oxidation, respectively. However, there was no apparent enhancement observed for doubly-doped TiO_2 materials for phenol photo-degradation.

It is worth mentioning that photocatalytic activities of MM-TiO_2 were observed substrate-dependent and were not correlated with any physicochemical property of MM-TiO_2. Neither absorption spectra in the visible region nor the crystal structures (anatase and rutile) of MM-TiO_2 appeared to play an important role in the visible-light induced photocatalytic reactions. For example, Pt(IV)-Cr-TiO_2, which was expected more efficient absorption of visible-light than Pt(II)-Cr-TiO_2, showed less photocatalytic activities than Pt(II)-Cr-TiO_2 for both MB degradation and I^- oxidation. However, Pt(IV)-Cr-TiO_2 showed higher photocatalytic activity than Pt(II)-Cr-TiO_2 for phenol degradation. In addition, Pt(II)-V-TiO_2 that has larger visible-light absorption than Pt(II)-Ni-TiO_2 were less photo-active for MB degradation and I^- oxidation, as well. Similarly, structure (i.e., the fraction of rutile) in MM-TiO_2 did not affect to visible-light photocatalytic activities of MM-TiO_2. Pt(IV)-Cr-TiO_2 with a high relative rutile content and Pt(II)-Ni-TiO_2 with no rutile at all showed comparable photocatalytic activities for MB degradation. For I^- oxidation, Pt(II)-Ni-TiO_2 and Cr-Ni-TiO_2 also showed comparable photocatalytic activities to Pt(II)-Cr-TiO_2.

Conclusions

Two metal ions co-doped TiO_2 was prepared by adding Pt (Pt^{4+} and Pt^{2+}), Cr^{3+}, V^{3+}, and Ni^{2+} ions during sol-gel synthesis. The metal-ion dopants used in this study were effectively incorporated into TiO_2 lattice either in Ti(IV) sites or in interstitial sites. Single and double-ion doping changed some of the physicochemical properties such as the reactive surface area and photophysical response of pristine TiO_2. 0.3 at.% Pt-0.3 at.% Cr-TiO_2 (both Pt^{4+} and Pt^{2+}), 0.3 at.% Cr-0.3 at.% V-TiO_2, and 0.3 at.% Pt-0.3 at.%

V-TiO_2 samples lowered A-R phase transformation temperature, since the individual dopant used for co-doping also had enhancing effect on A-R phase transformation. However, 0.3 at.% Pt-0.3 at.% Ni-TiO_2 and 0.3 at.% Cr-0.3 at.% Ni-TiO_2 remained strictly in the anatase phase due to Ni co-doping although doping with Pt and Cr alone accelerated A-R phase transformation. All co-doped TiO_2 materials gave extended UV-vis absorption between 400 and 700 nm, but only 0.3 at.% Pt(IV)- 0.3 at.% Cr-TiO_2 enhanced visible-light absorption compared to singly-doped TiO_2. Visible-light photocatalytic activities were evaluated for the degradation of MB, phenol and the oxidation of I^- in aqueous solution. The photocatalytic activities of co-doped TiO_2 strongly depended on the nature of the electron-donating substrate and were not correlated with any physicochemical property of the co-doped TiO_2. Pt-Cr-TiO_2 and Pt-Ni-TiO_2 enhanced the rate of MB degradation while Pt-Cr-TiO_2, Cr-V-TiO_2, Pt-Ni-TiO_2, and Cr-Ni-TiO_2 showed enhanced activity for I^- oxidation. However, none of the co-doped samples showed enhanced photocatalytic activity for phenol degradation compared to their singly-doped TiO_2 counterparts. All co-doped TiO_2 samples exhibited some enhancement in photo-catalytic activity for all three reactions compared to undoped nano-particulate TiO_2.

Acknowledgement

We are grateful to the Hydrogen Energy Research & Development Center and 21st Century Frontier Research and Development Program of the Ministry of Science and Technology of Korea for research support.

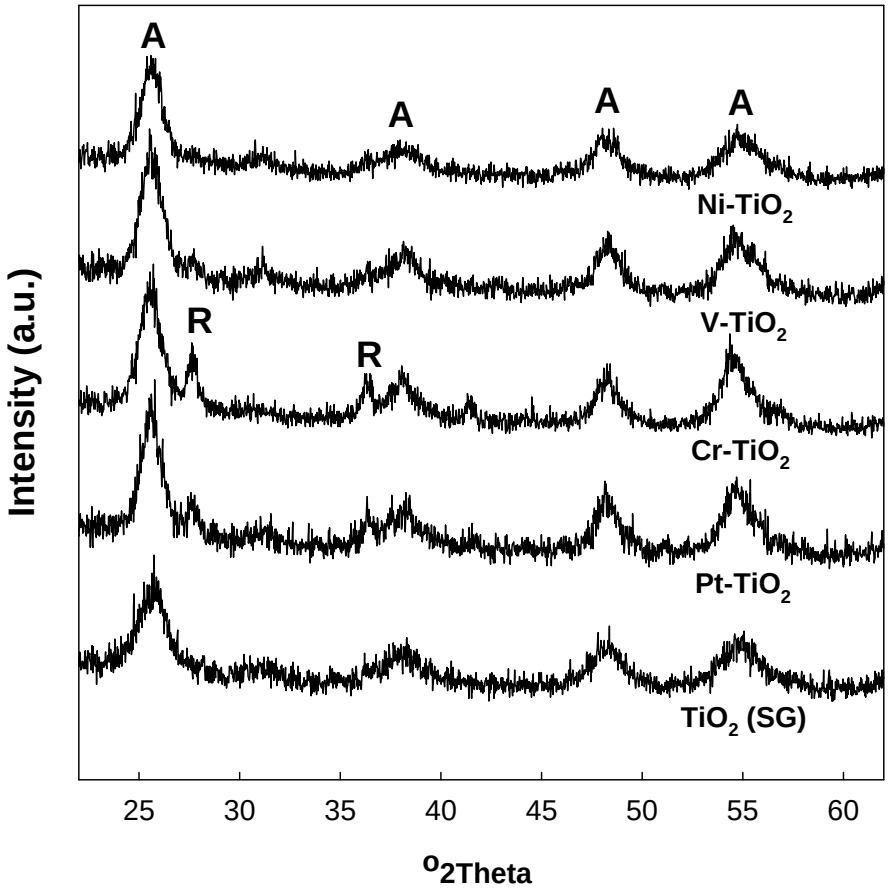

Figure 3.1. X-ray diffraction (XRD) pattern measured for 0.3 at.% M-TiO_2 prepared at 400 ^{o}C. (A: anatase phase, R: rutile phase)

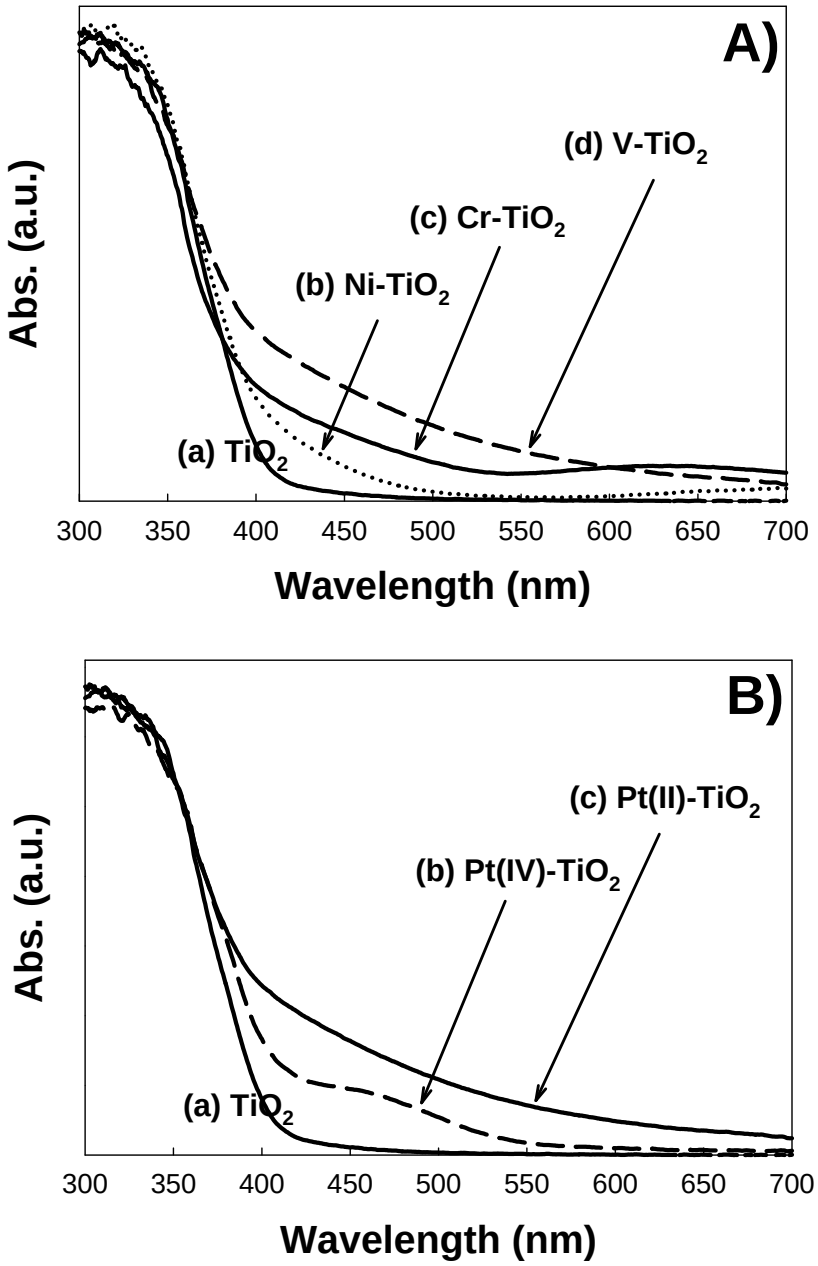

Figure 3.2. UV/vis diffuse reflectance spectra (DRS) for 0.3 at.% M-TiO_2 samples: A) undoped TiO_2, Cr-TiO_2, Ni-TiO_2, and V-TiO_2. B) Pt(IV)-TiO_2 and Pt(II)-TiO_2

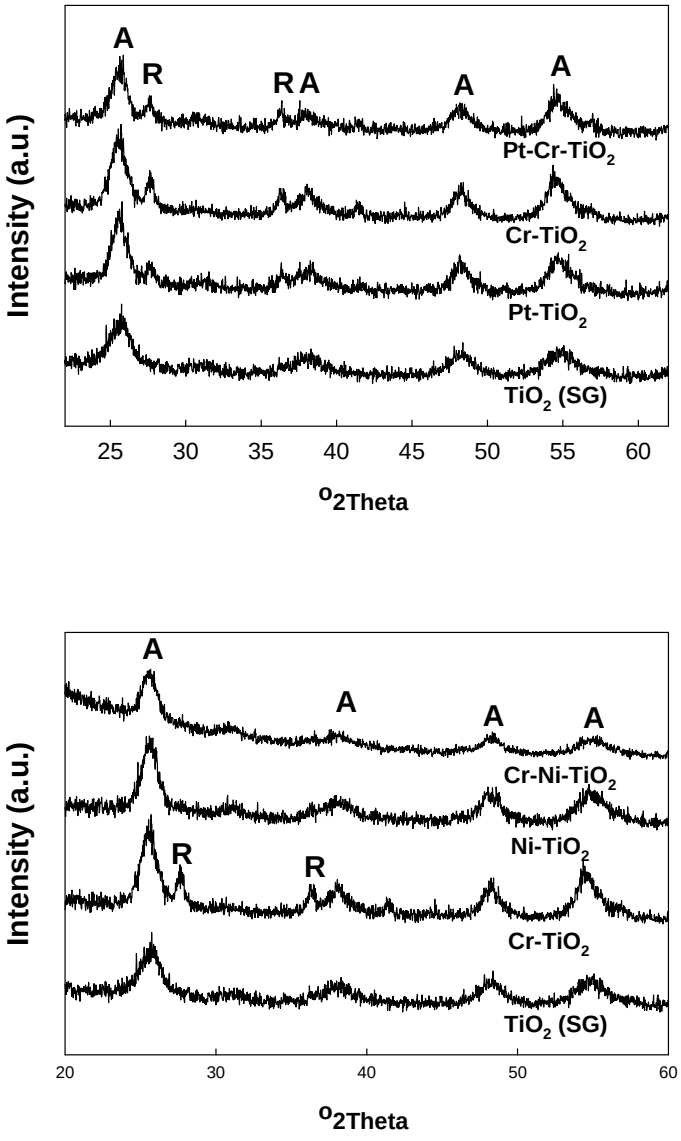

Figure 3.3. X-ray diffraction (XRD) pattern measured for 0.3 at.% Pt-Cr-TiO_2 and Cr-Ni-TiO_2. (A: anatase phase, R: rutile phase)

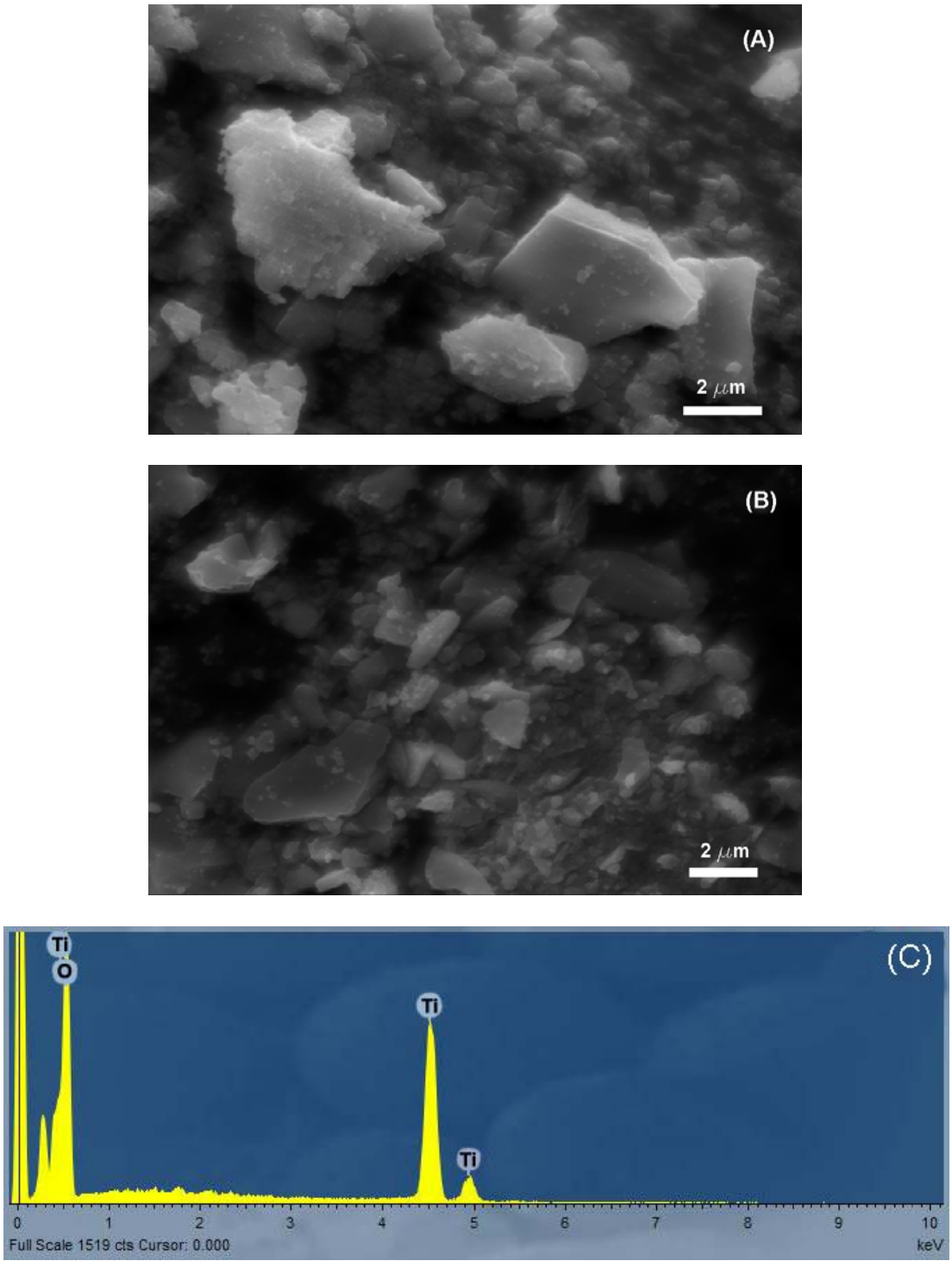

Figure 3.4. SEM images of (a) 0.3 at.% Pt(IV)-Cr-TiO_2, (b) 0.3 at.% Pt(II)-Cr-TiO_2 and EDS spectra of Pt(II)-Ni-TiO_2 (c) that clearly shows dopants signals (i.e., Pt and Ni) other than Ti and O signals were not observed.

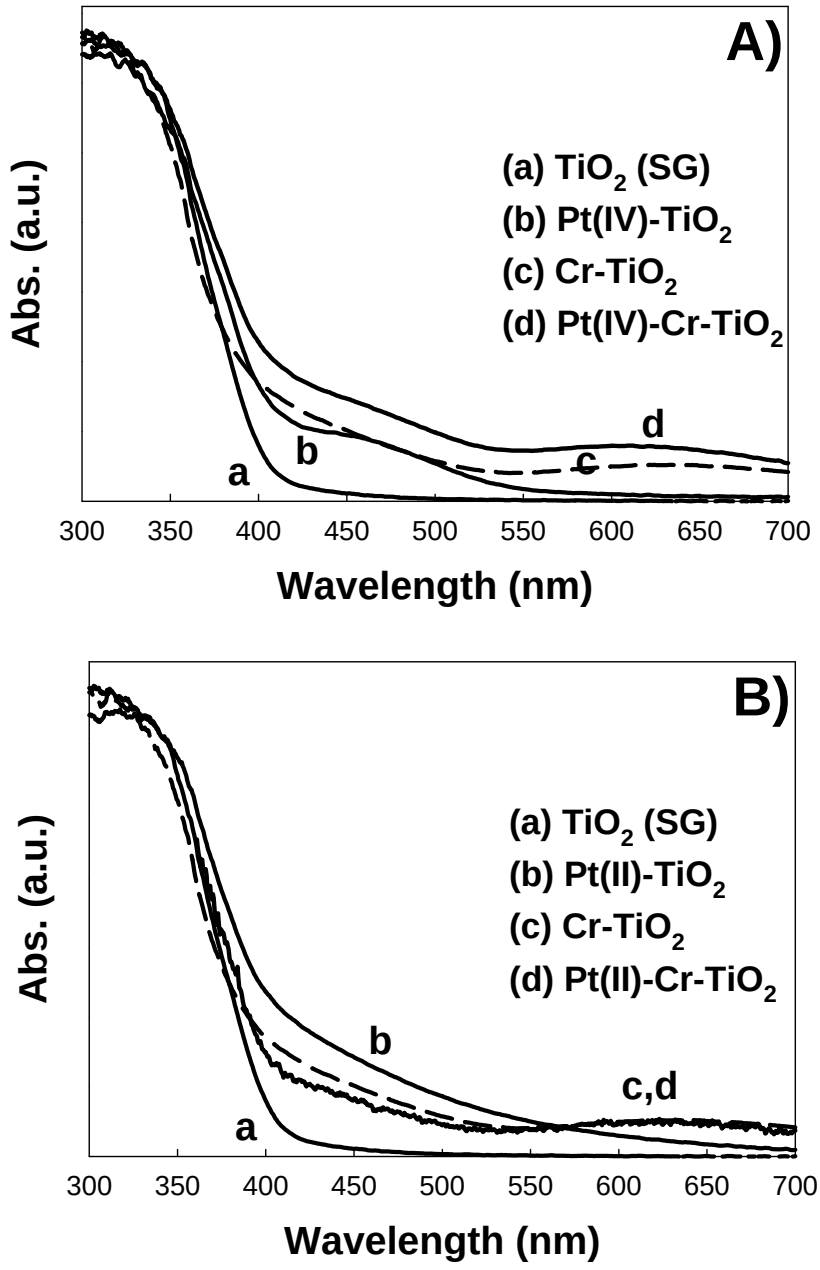

Figure 3.5. UV/vis diffuse reflectance spectra (DRS) for 0.3 at.% Pt-Cr-TiO_2: A) Pt(IV)-Cr-TiO_2, B) Pt(II)-Cr-TiO_2 samples

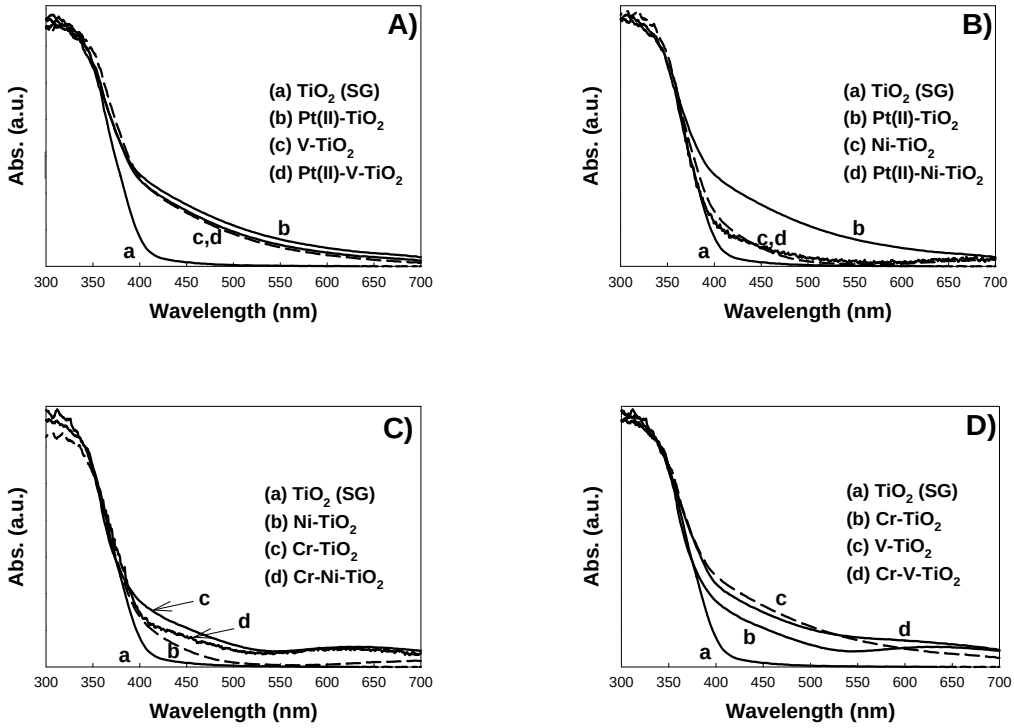

Figure 3.6. UV/vis diffuse reflectance spectra (DRS) for A) 0.3 at.% Pt(II)-V-TiO_2, B) 0.3 at.% Pt(II)-Ni-TiO_2, C) 0.3 at.% Cr-Ni-TiO_2, D) 0.3 at.% Cr-V-TiO_2

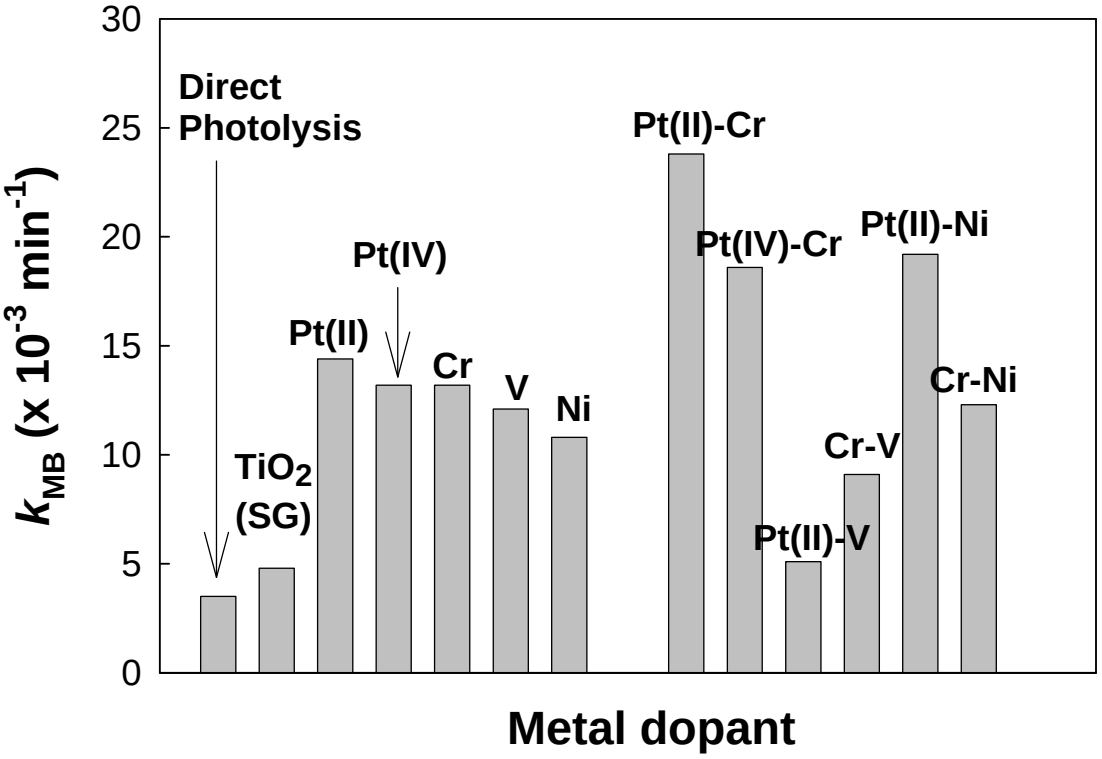

Figure 3.7. The comparison of degradation rate constant (k_{MB}) of MB for various single-doped or co-doped TiO_2 samples (0.3 at.% doping)

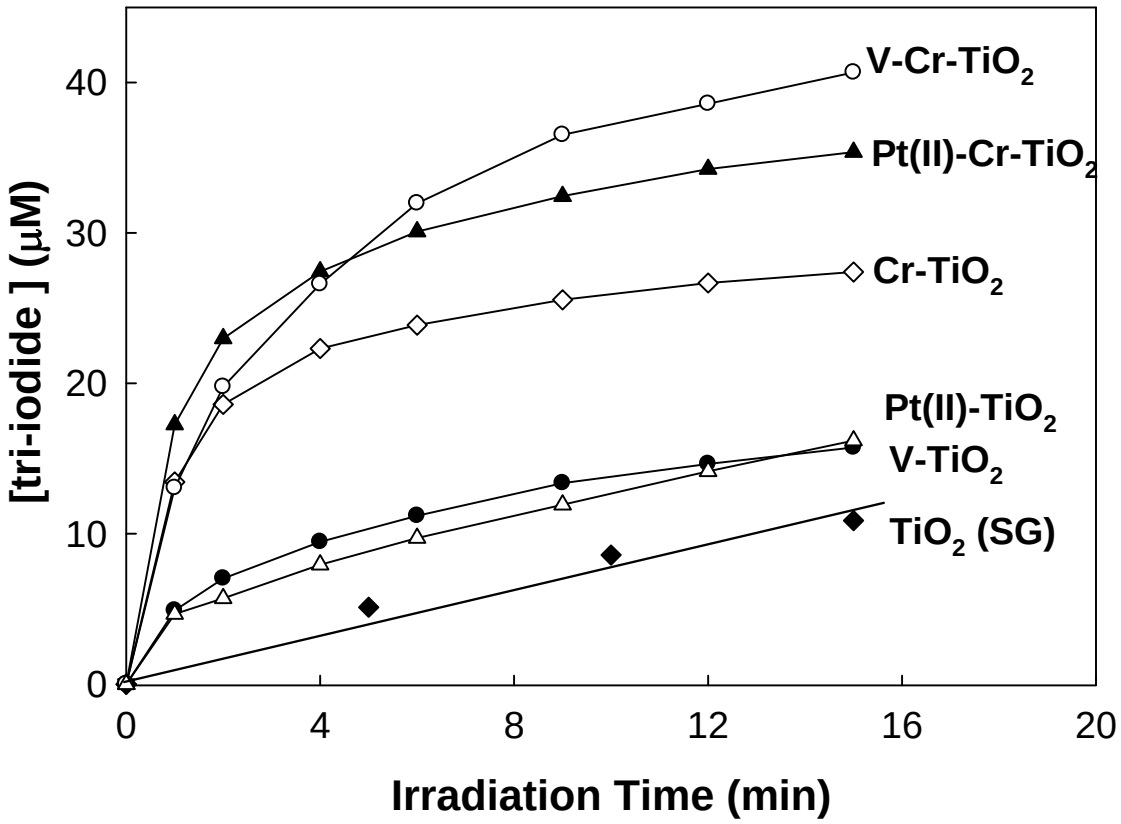

Figure 3.8. The production of tri-iodide by iodide oxidation ($[I^-]_0$ = 50 mM, total volume = 30 mL) with selected MM-TiO_2 (0.3 at.% doping level, 1 g/L) under visible-light irradiation (500 W, > 400 nm)

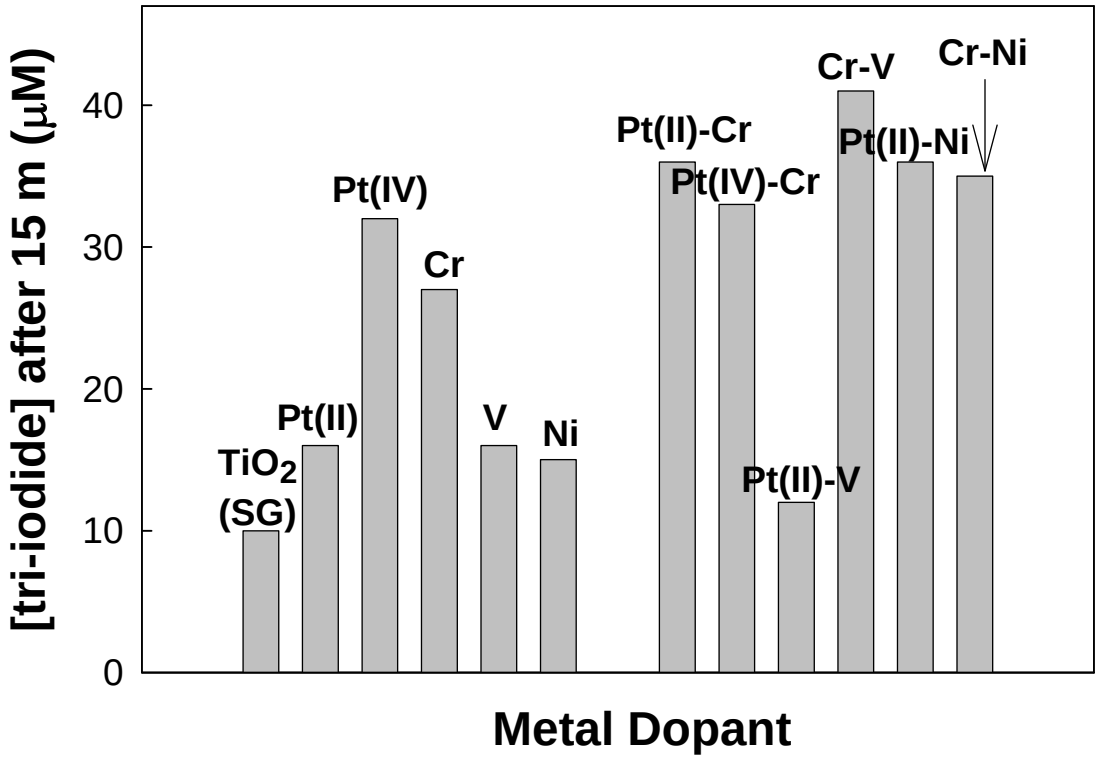

Figure 3.9. The comparison of various single-doped or co-doped TiO_2 samples (0.3 at.% doping) for I^- oxidation

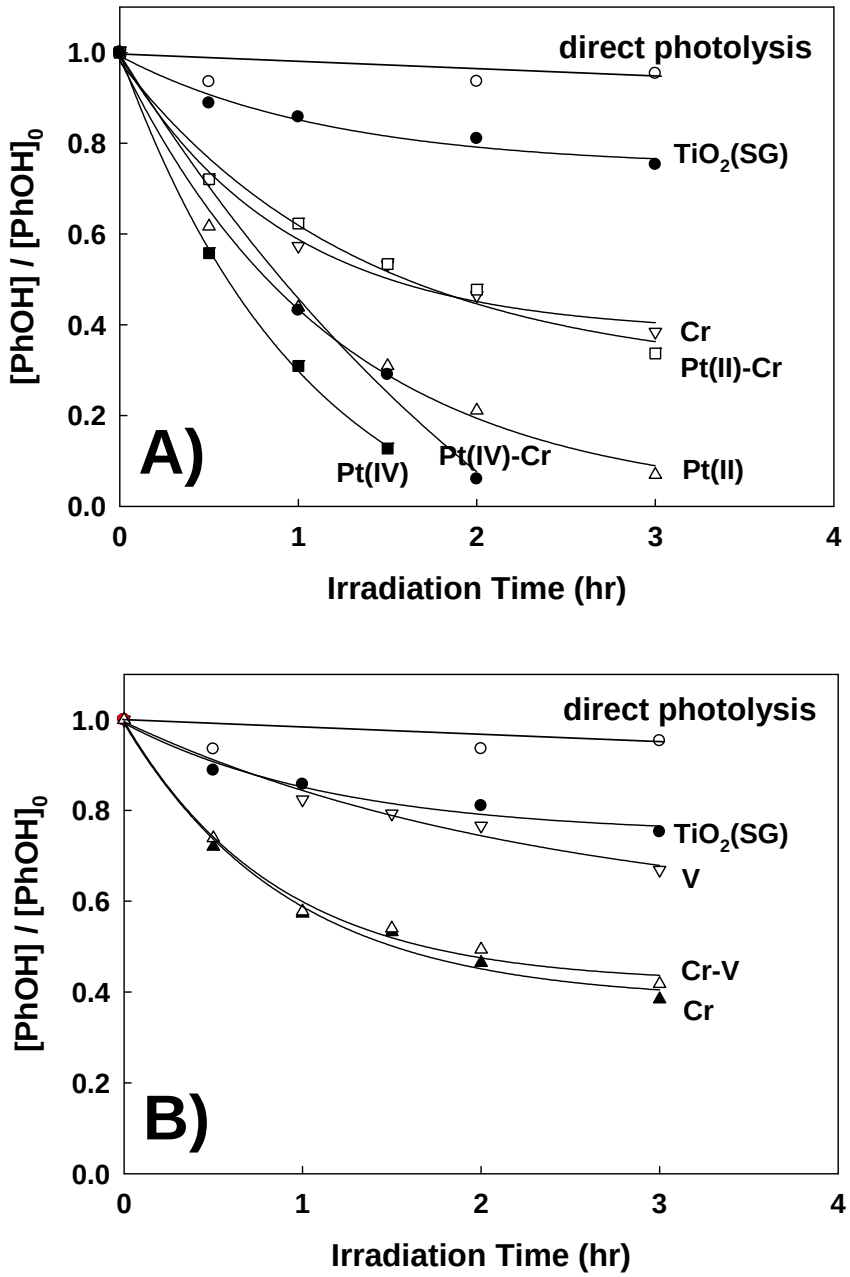

Figure 3.10. The degradation of phenol ($[phenol]_0$ = 50 μM, 1 g/L of 0.3 at.% single-doped or co-doped-TiO_2, > 400 nm): A) Pt-Cr-TiO_2, (B) Cr-V-TiO_2

TABLE 3.1. Characterization of MM-TiO_2 photocatalysts at 0.3 at.% doping level

Sample	Color	Surface Area (m^2g^{-1})	Crystal structure (X_R %)
TiO_2 (SG)	White	104	Anatase (0)
Pt(II)-TiO_2	Light brown	111	Anatase/Rutile (22)
Pt(IV)-TiO_2	Light brown	106	Anatase/Rutile (26)
Cr-TiO_2	Green	115	Anatase/Rutile (34)
V-TiO_2	Orange	132	Anatase/Rutile (13)
Ni-TiO_2	Green	112	Anatase (0)
Pt(II)-Cr-TiO_2	Dark green	112	Anatase/Rutile (30)
Pt(IV)-Cr-TiO_2	Dark green	108	Anatase/Rutile (32)
Cr-V-TiO_2	Brown	115	Anatase/Rutile (28)
Pt(II)-V-TiO_2	Brown	118	Anatase/Rutile (24)
Pt(II)-Ni-TiO_2	Light green	110	Anatase (0)
Cr-Ni-TiO_2	Green	115	Anatase (0)

TABLE 3.2. Photocatalytic activities of Pt(II)-Cr-TiO_2 with different doping level for I^- oxidation under visible-light irradiation (> 400 nm)

Sample	$[I_3^-]_{prod.}$ (μM) after 15 min
0.3 % Pt(II) with	
0 % Cr	16
0.1 % Cr	19
0.2 % Cr	21
0.3 % Cr	36
0.5 % Cr	32
0.3 % Cr with	
0 % Pt	29
0.1 % Pt	31
0.2 % Pt	28
0.3 % Pt	36
0.5 % Pt	32

References

(1) Asahi, R.; Morikawa, T.; Ohwaki, T.; Aoki, K.; Taga, Y. *Science* **2001**, *293*, 269.

(2) Mrowetz, M.; Balcerski, W.; Colussi, A. J.; Hoffman, M. R. *J. Phys. Chem. B* **2004**, *108*, 17269.

(3) Sauthier, G.; Gyorgy, E.; Figueras, A. *J. Mater. Res.* **2008**, *23*, 2340.

(4) Umebayashi, T.; Yamaki, T.; Tanaka, S.; Asai, K. *Chem. Lett.* **2003**, *32*, 330.

(5) Su, W. Y.; Zhang, Y. F.; Li, Z. H.; Wu, L.; Wang, X. X.; Li, J. Q.; Fu, X. Z. *Langmuir* **2008**, *24*, 3422.

(6) Liu, G.; Chen, Z. G.; Dong, C. L.; Zhao, Y. N.; Li, F.; Lu, G. Q.; Cheng, H. M. *J. Phys. Chem. B* **2006**, *110*, 20823.

(7) Hong, X. T.; Wang, Z. P.; Cai, W. M.; Lu, F.; Zhang, J.; Yang, Y. Z.; Ma, N.; Liu, Y. J. *Chem. Mater.* **2005**, *17*, 1548.

(8) Zhou, J. K.; Lv, L.; Yu, J. Q.; Li, H. L.; Guo, P. Z.; Sun, H.; Zhao, X. S. *J. Phys. Chem. C* **2008**, *112*, 5316.

(9) Zhang, X. W.; Lei, L. C. *Mater. Lett.* **2008**, *62*, 895.

(10) Zhang, X. W.; Zhou, M. H.; Lei, L. C. *Catal. Commun.* **2006**, *7*, 427.

(11) Teoh, W. Y.; Amal, R.; Madler, L.; Pratsinis, S. E. *Catal. Today* **2007**, *120*, 203.

(12) Iketani, K.; Sun, R. D.; Toki, M.; Hirota, K.; Yamaguchi, O. *Mater. Sci. Eng., B* **2004**, *108*, 187.

(13) Klosek, S.; Raftery, D. *J. Phys. Chem. B* **2001**, *105*, 2815.

(14) Wu, J. C. S.; Chen, C. H. *J. Photochem. Photobiol., A* **2004**, *163*, 509.

(15) Borgarello, E.; Kiwi, J.; Gratzel, M.; Pelizzetti, E.; Visca, M. *J. Am. Chem. Soc.* **1982**, *104*, 2996.

(16) Anpo, M.; Ichihashi, Y.; Takeuchi, M.; Yamashita, H. *Sci. Technol. Catal.* **1999**, *121*, 305.

(17) Kim, D. H.; Lee, K. S.; Kim, Y. S.; Chung, Y. C.; Kim, S. J. *J. Am. Ceram. Soc.* **2006**, *89*, 515.

(18) Kim, S.; Hwang, S. J.; Choi, W. Y. *J. Phys. Chem. B* **2005**, *109*, 24260.

(19) Park, H.; Choi, W.; Hoffmann, M. R. *J. Mater. Chem.* **2008**, *18*, 2379.

(20) Bae, E.; Choi, W. *Environ. Sci. Technol* **2003**, *37*, 147.

(21) Choi, W. Y.; Termin, A.; Hoffmann, M. R. *J. Phys. Chem.* **1994**, *98*, 13669.

(22) Chen, J. H.; Yao, M. S.; Wang, X. L. *J. Nano. Res.* **2008**, *10*, 163.

(23) Di Paola, A.; Garcia-Lopez, E.; Ikeda, S.; Marci, G.; Ohtani, B.; Palmisano, L. *Catal. Today* **2002**, *75*, 87.

(24) Srinivasan, S. S.; Wade, J.; Stefanakos, E. K.; Goswami, Y. *J. Alloys Compd.* **2006**, *424*, 322.

(25) Ahmad, A.; Shah, J. A.; Buzby, S.; Shah, S. I. *Eur. J. Inorg. Chem.* **2008**, 948.

(26) Kato, H.; Kudo, A. *J. Phys. Chem. B* **2002**, *106*, 5029.

(27) Niishiro, R.; Kato, H.; Kudo, A. *Phys. Chem. Chem. Phys.* **2005**, *7*, 2241.

(28) Niishiro, R.; Konta, R.; Kato, H.; Chun, W. J.; Asakura, K.; Kudo, A. *J. Phys. Chem. C* **2007**, *111*, 17420.

(29) Huang, D. E.; Liao, S. J.; Quan, S. Q.; Liu, L.; He, Z. J.; Wan, J. B.; Zhou, W. B. *J. Mater. Res.* **2007**, *22*, 2389.

(30) Li, D.; Haneda, H.; Hishita, S.; Ohashi, N. *Chem. Mater.* **2005**, *17*, 2588.

(31) Yu, J. G.; Zhou, M. H.; Cheng, B.; Zhao, X. J. *J. Mol. Cat. A: Chem.* **2006**, *246*, 176.

(32) Liu, H. Y.; Gao, L. *J. Am. Ceram. Soc.* **2004**, *87*, 1582.

(33) Sakatani, Y.; Ando, H.; Okusako, K.; Koike, H.; Nunoshige, J.; Takata, T.; Kondo, J. N.; Hara, M.; Domen, K. *J. Mater. Res.* **2004**, *19*, 2100.

(34) Sakatani, Y.; Nunoshige, J.; Ando, H.; Okusako, K.; Koike, H.; Takata, T.; Kondo, J. N.; Hara, M.; Domen, K. *Chem. Lett.* **2003**, *32*, 1156.

(35) Pan, C. C.; Wu, J. C. S. *Mater. Chem. Phys.* **2006**, *100*, 102.

(36) Kim, S.; Lee, S.-K. *J. Photochem. Photobiol. A-Chem.* **2009**, *203*, 145.

(37) Zhao, Z. Y.; Liu, Q. J. *Catal. Lett.* **2008**, *124*, 111.

(38) Wang, Y.; Meng, Y. L.; Ding, H. M.; Shan, Y. K.; Zhao, X.; Tang, X. Z. *J. Phys. Chem. C* **2008**, *112*, 6620.

(39) He, Z. Q.; Xu, X.; Song, S.; Xie, L.; Tu, J. J.; Chen, J. M.; Yan, B. *J. Phys. Chem. C* **2008**, *112*, 16431.

(40) Shannon, R. D. *Acta Crystallogr., Sec. A* **1976**, *32*, 751.

(41) Serpone, N.; Lawless, D.; Disdier, J.; Herrmann, J. M. *Langmuir* **1994**, *10*, 643.

(42) Umebayashi, T.; Yamaki, T.; Itoh, H.; Asai, K. *J. Phys. Chem. Solids* **2002**, *63*, 1909.

(43) Kudo, A.; Niishiro, R.; Iwase, A.; Kato, H. *Chem. Phys.* **2007**, *339*, 104.

(44) Kuznetsov, V. N.; Serpone, N. *J. Phys. Chem. B* **2006**, *110*, 25203.

(45) Serpone, N. *J. Phys. Chem. B* **2006**, *110*, 24287.

(46) Lisachenko, A. A.; Kuznetsov, V. N.; Zakharov, M. N.; Mikhailov, R. V. *Kinet. Catal.* **2004**, *45*, 189.

(47) Kuznetsov, V. N.; Krutitskaya, T. K. *Kinet. Catal.* **1996**, *37*, 446.

(48) Spurr, R. A.; Myers, H. *Anal. Chem.* **1957**, *29*, 760.